Enhancement of Electrode Stability using Platinum-Cobalt Nanocrystals on a Novel Composite SiCTiC Support

María Millán, Héctor Zamora, Manuel A. Rodrigo and Justo Lobato,*

Chemical Engineering Department, Faculty of Chemical Sciences and Technologies, University of Castilla-La Mancha, Enrique Costa Novella, Av. Camilo Jose Cela n 12, Ciudad Real, Spain

*Corresponding author. Tel: +34926 295 300; fax: +34 926 295 256. E-mail address: justo.lobato@uclm.es

Keywords

Carbides, Pt alloys, stability, HT-PEMFCs, oxygen reduction reaction

Abstract

PtCo alloy catalysts for high temperature PEMFCs (Protonic Exchange Membrane Fuel Cells) were synthesized on a novel non-carbonaceous support (SiCTiC) using the impregnation method with $NaBH_4$ as the reducing agent at different synthesis temperatures to evaluate the effect of this variable on their physicochemical and electrochemical properties. The catalysts were characterized by inductively coupled plasma optical emission spectrometry (ICP-OES), scanning electron microscopy-energy dispersive X-ray spectroscopy (SEM-EDX), X-ray diffraction (XRD), transmission electron microscope-energy dispersive X-ray (TEM) and temperature programmed reduction (TPR). In addition, the electrochemical characterization (i.e., cyclic voltammetry (CV), oxygen reduction reaction (ORR) and chronoamperometry) was carried out with a rotating disk electrode (RDE). For the cyclic voltammetry investigation, 400 cycles were performed in hot phosphoric acid and a half-cell to evaluate the stability

of the synthesized catalysts. The catalyst synthesized on SiCTiC exhibited excellent durability compared to the catalyst synthesized on a Vulcan support. In addition, all synthesized catalysts exhibited better catalytic activity than that of the PtCo/C catalysts. The best results were observed for the catalyst synthesized at 80 °C due to its shorter Pt-Pt nearest-neighbor and higher alloy degree. Finally, a preliminary stability test was conducted in an HT-PEMFC, and promising results in terms of stability and performance were observed.

1. Introduction

The increasing concerns surrounding global warming, the energy crisis and air pollution have increased research efforts on new alternative energy sources[1-2]. Polymer electrolyte membrane fuel cells (PEMFCs) are a promising device for the conversion of chemical energy from a fuel, such as hydrogen, directly into electricity with high energy efficiency, high power density and low environmental impact[3-4]. Among the PEM fuel cells, the cells that operate at a high temperature are very promising. The use of this cell significantly increases the CO tolerance, enhances the oxygen reduction reaction kinetics and decreases the thermal and water management of the system[5-9]. However, durability issues, cost reduction and fuel cell performance improvements are the main challenges for the widespread application of this technology in the market.

Several catalyst supports have been studied for application as anode and cathode electrodes in PEMFCs by Sharma et al.[10]. The numerous material supports can be classified as carbonaceous and non-carbonaceous. Carbon black is commonly used as a support in PEM fuel cells. However, this carbonaceous support exhibits high corrosion. Therefore, the development of new materials that decrease the corrosion degree while maintaining good conductivity is necessary[10]. Recently, several novel ceramic materials,

such as tungsten carbide[11], titanium-based materials[12-14] and silicon carbide[15-18], have been evaluated as catalyst supports to improve the service lifetime of the catalytic layer. The use of a non-carbonaceous support, such a SiCTiC, resulted in better thermal and electrochemical resistance than the carbon material under the same operating conditions[19].

In regards to the metal catalyst, platinum has been the most used metal in this type of fuel cells. Nevertheless, the scarcity and high cost of this metal is a hindrance, and new materials that decrease the cost without compromising the catalytic activity would be beneficial[20-22]. Therefore, binary and ternary Pt-alloys that exhibit a higher activity than Pt alone have been developed[23-25]. The use of alloys results in an improvement in the oxygen reduction reaction (ORR) due to different structural changes caused by alloying (i.e., modifications in the geometrical[26] (decrease in the Pt-Pt bond distance) or electronic[27] (increase in the Pt d-electron vacancy) structure of platinum metal). Therefore, PtM alloys could increase the rate of the oxygen reduction reaction, which is one of the main challenges in this type of fuel cell[28]. Furthermore, the catalytic activity of the Pt-based catalysts is influenced by their structure, metal particle size and shape and the supporting material used on the electrode[29-32].

In this study, binary PtCo alloy catalysts supported on a novel non-carbonaceous support (SiCTiC) have been synthesized using an impregnation method with $NaBH_4$ as the reducing agent. The effect of temperature (30, 50 and 80 °C) during the synthesis was investigated. All obtained samples were physically and chemically characterized using ICP, XRD, SEM, TEM and TPR. In addition, a rotating disk electrode (RDE) was used to gain insight into the kinetics and mechanism of the O_2 reduction reaction and the electrochemical active surface area of the catalysts. Furthermore, the electrodes were prepared to evaluate their stability in a half-cell with catalysts synthesized at different

temperatures. Finally, electrodes for the high temperature PEMFC were prepare for use as a cathode in this type of fuel cell, and the experiments were performed with phosphoric acid-doped PBI membranes, which are good electrolytes for this type of technology[8, 33].

2. Experimental

2.1. Synthesis of Pt-Co catalysts

PtCo nanocrystal catalysts were prepared using two different methods. The first approach employed the formic acid method (FAM), which consists of deposition of precursor salts using formic acid as a reducing agent[19]. The second approach employed an impregnation method using $NaBH_4$ as the reducing agent. SiCTiC (90:10 mol ratio) was used as a support (provided by SICAT, Paris; France), and $H_2PtCl_6 \cdot 6H_2O$ and $Cl_2Co \cdot 6H_2O$ were employed as precursor salts (Sigma-Aldrich). The mixture was suspended in deionized water and stirred at different temperatures to evaluate the influence of this variable on the physicochemical and electrochemical properties. Once the set temperature was reached, 20 ml of $NaBH_4$ per gram of metal were added to the suspension. The amount of the metal precursor was adjusted to achieve a Pt:Co molar ratio of 1:1, and the total metal content in the catalysts was 40 wt%. The resulting black precipitate was filtered and washed with deionized water at 80 °C. Finally, the solid was dried in a vacuum oven at 90 °C for 12 h.

2.2. Characterization

The metal loading and molar ratio of both metals were determined by inductively coupled plasma optical emission spectrometry (ICP-OES) using a Varian Liberty RL spectrometer. The X-ray diffraction (XRD) measurements were carried out on a Philips PW-1700 diffractometer using Cu Kα radiation. The 2θ angular regions between 20° and 90° were explored at a scan rate of 0.1 ° s^{-1}. In addition, the samples were characterized

by SEM-EDX using a Jeol 6490LV. The morphology and particle size distribution of the PtCo catalysts were determined using a Joel 2100 transmission electron microscope (TEM). Furthermore, the presence of surface oxides was evaluated by temperature programmed reduction analysis. The reduction of the catalyst was carried out under a stream of hydrogen (5 vol%) diluted with Ar at a flow rate of 20 mL min^{-1}. The temperature was increased at a heating rate of 5 °C min^{-1} up to 900 °C.

2.3. Preparation of inks

Different catalyst inks were prepared to investigate the catalytic stability. The first ink was prepared for use in an RDE, and the second ink was employed for preparing electrodes that were used in the half-cell and single cell.

The catalyst inks for the RDE were prepared by sonicating the catalyst and Nafion in a water-propanol mixture. 2 mg of the catalyst and 8 μL of Nafion (Sigma-Aldrich, 5 wt. %) were mixed and stirred for 1 min. Then, 200 μL of isopropanol and 800 μL of deionized water were added and sonicated for 30 min. The working electrode consisted of a glassy-carbon rotating disk electrode (0.196 cm^2). 20 μL of the catalyst ink was dropped onto the working electrode and dried in a N_2 flow.

Next, electrodes with 0.3 mg $_{Pt\text{-}Co}$ cm^{-2} and 0.6 mg $_{Pt\text{-}Co}$ cm^{-2} were prepared for use in a half-cell and single cell, respectively. The inks were prepared using N, N' - dimethylacetamide (DMAc (1-20 PBI/support ratio)) as a dispersing solvent and polybenzimidazole (PBI, 1.5 wt. %) as a binder. The first ink was spread over 4 cm^2 on the surface of carbon paper for the half-cell test and heated at 190 °C for 2 h to eliminate any remaining solvent.

2.4. MEA preparation

A catalyst layer was deposited by spraying the catalyst ink over the commercial electrodes (Freudenberg Vliesstoffe, H23C2). The catalyst ink for the cathode and anode electrodes was prepared from the 40% wt. PtCo/SiCTiC and PtCo/Vulcan catalysts synthesized at 80 °C and a commercial 40% wt. Pt/C catalyst, respectively. This metal amount on the catalyst powder was fixed based on the optimization results for the catalyst layer in HT-PEMFCs, which was previous reported by our research group[33] and in agreement with the ratios employed in previously reported studies[34]. In all cases, the Pt and PtCo loading on the two electrodes (anode and cathode) was 0.6 mg_{Pt} cm^{-2}. After deposition of the catalyst layer, the electrodes were dried at 190 °C for 2 h to remove the remaining DMAc. Then, a 10 wt. % phosphoric acid solution was dropped on the electrode surface to dope the PBI into the catalytic layer. The electrodes were left to absorb the acid for one day. To prepare the MEA, a PBI membrane was doped in 85 wt. % PA at room temperature for 5 days to achieve good proton conductivity. The doping level acquired by the membrane was approximately 9 molecules of acid per polymer repeating unit. The corresponding thickness of the doped membrane was 83.2 μm. The superficial acid on the membrane was thoroughly wiped off with filter paper, and the membrane was used to prepare the MEA. To fabricate the MEA, the doped membrane was sandwiched between a couple of electrodes, and the whole system was hot-pressed at 130 °C and 1 MPa for 15 min. The completed MEA was inserted into the cell between bipolar plates of graphite (with a five serpentine channels frame in each plate). The geometric area of each electrode was 25 cm^2.

2.5. Electrochemical measurements

All electrochemical measurements were carried out on an Autolab potentiostat/galvanostat (PGSTAT-302N). Pure Au foil and Ag/AgCl electrodes were used as the counter and reference electrode, respectively, in the RDE and half-cell tests.

145

146 *2.5.1. Rotating disk electrode tests*

147 To evaluate the ECSA (electrochemical surface area)[33, 35-36], cyclic voltammetry
148 was performed between -0.2 and 1 V at a scan rate of 50 mV s^{-1}. The rotation rate was
149 1500 rpm, and the system was maintained in an inert atmosphere containing N_2. Then,
150 the oxygen reduction reactions were performed using different rotation rates (400, 800,
151 1200 and 1600 rpm) to evaluate the activity and kinetics of this reaction. In this case, the
152 system was saturated in O_2, and the ORR was performed between 0.1 and 0.9 V using a
153 scan rate of 4 mV s^{-1}. Finally, a chronoamperometric analysis was carried out to assess
154 the degradation suffered by the catalysts at a constant potential (0.55 V) and 1000 rpm.
155 The analyses were performed in 0.5 M H_2SO_4, which was used as a proton generator.

156 *2.5.2. Half-cell tests*

157 To evaluate the electrochemical stability of the catalysts, various 1.5 cm^2 diameter
158 electrodes were prepared using the same method as that employed during the MEA
159 electrode preparation with a targeted Pt loading of 0.3 mg cm^{-2}. Then, 400 cycles were
160 performed in 2 M phosphoric acid media to approximately the conditions of the HT-PEM
161 fuel cell environment between -0.2-1 V vs Ag/AgCl at 50 mV s^{-1}. The system was
162 maintained under an inert atmosphere containing N_2. In addition, the medium was heated
163 at 50 °C to approximate to the cell conditions and simultaneously promote catalyst
164 degradation. A schematic diagram of the half-cell that was used to perform the
165 electrochemical tests has been reported elsewhere [37].

166 *2.5.3. Fuel cell characterization*

167 The MEAs that prepared with thermally cured PBI membranes were mounted and
168 characterized in a commercially available cell compression unit (CCU) that was provided
169 by Baltic fuel cells GmbH (Germany). The break-in procedure consisted of operating at
170 0.1 A cm^{-2} and a λ (H_2 / O_2 ratio) of 1.5/9.5 for 60 h. A preliminary stability test was
171 conducted by increasing the current density to 0.2 A cm^{-2} (160 °C) while working at
172 constant stoichiometric coefficients (λ_{H2} of 1.5 and λ_{O2} of 9.5). For further
173 characterization, galvanostatic polarization curves were recorded every 48 h since the
174 final step of the break-in procedure according to a previously reported[38]. These tests were
175 performed from the OCV to 0.4 V with air at a constant $\lambda_{H2/O2}$ of 1.5/2 and then with
176 oxygen at a constant $\lambda_{H2/O2}$ of 1.5/9.5. Therefore, this preliminary life test was performed
177 under accelerate stress conditions.

178 ## 3. Results and discussion

179 ### 3.1. Physicochemical characterization

180 The synthesized catalysts were physicochemically characterized using previously
181 reported techniques. First, the formic method was used to produce the electrocatalysts to
182 evaluate the effect of the addition of Co to Pt/SiCTiC because this method was previously
183 used by our research group[19]. However, this method cannot reduce the cobalt precursor
184 salt. Therefore, this method does not allow us to prepare PtCo catalysts. Then, the
185 impregnation method using sodium borohydride as a reducing agent was performed as
186 stated in the experimental section. Initially, the ICP measurements were carried out to
187 evaluate the amount of metal deposited on the support. Table 1 shows the weight
188 percentages of Pt and Co and the obtained molar ratios for the samples synthesized at
189 different temperatures using the $NaBH_4$ method based on the ICP and EDX-SEM
190 analyses. The experimental Pt/Co molar ratio was double the desired nominal rate. To
191 evaluate the influence of the catalytic support on the metal loading and alloy composition,

an additional 1:1 PtCo-based catalyst was prepared using Vulcan XC72 as the catalyst support. 34.9 and 5.7 wt. % Pt and Co, respectively, were obtained in an atomic ratio of approximately 2. Therefore, the PtCo atomic ratio was not influenced by the catalytic support. Next, the differences between the theoretical and observed PtCo atomic ratios may be due to a competitive effect during the reduction process. Co^{2+} ions may not have an equal chance of being reduced when the process occurs in the presence of $PtCl_6^{2-}$ ions in solution[39]. Furthermore, Figure 1 shows the SEM images and the EDX spectra of the PtCo(1:1)/SiCTiC catalysts synthesized at different temperatures. Based on the SEM analysis, the obtained atomic ratios were similar to those obtained from ICP, as shown in Table 1.

Table 1. Data obtained from ICP and EDX-SEM analyses.

	ICP results			SEM results		
Synthesis temperature	wt. % Pt	wt. % Co	Pt/Co atomic	wt. % Pt	wt. % Co	Pt/Co atomic
30 °C	38.6	5.6	68:32	38.2	5.5	68:32
50 °C	34.8	5.3	66:34	34.8	5.3	66:34
80 °C	34.6	5.3	66:34	34.6	5.2	67:33

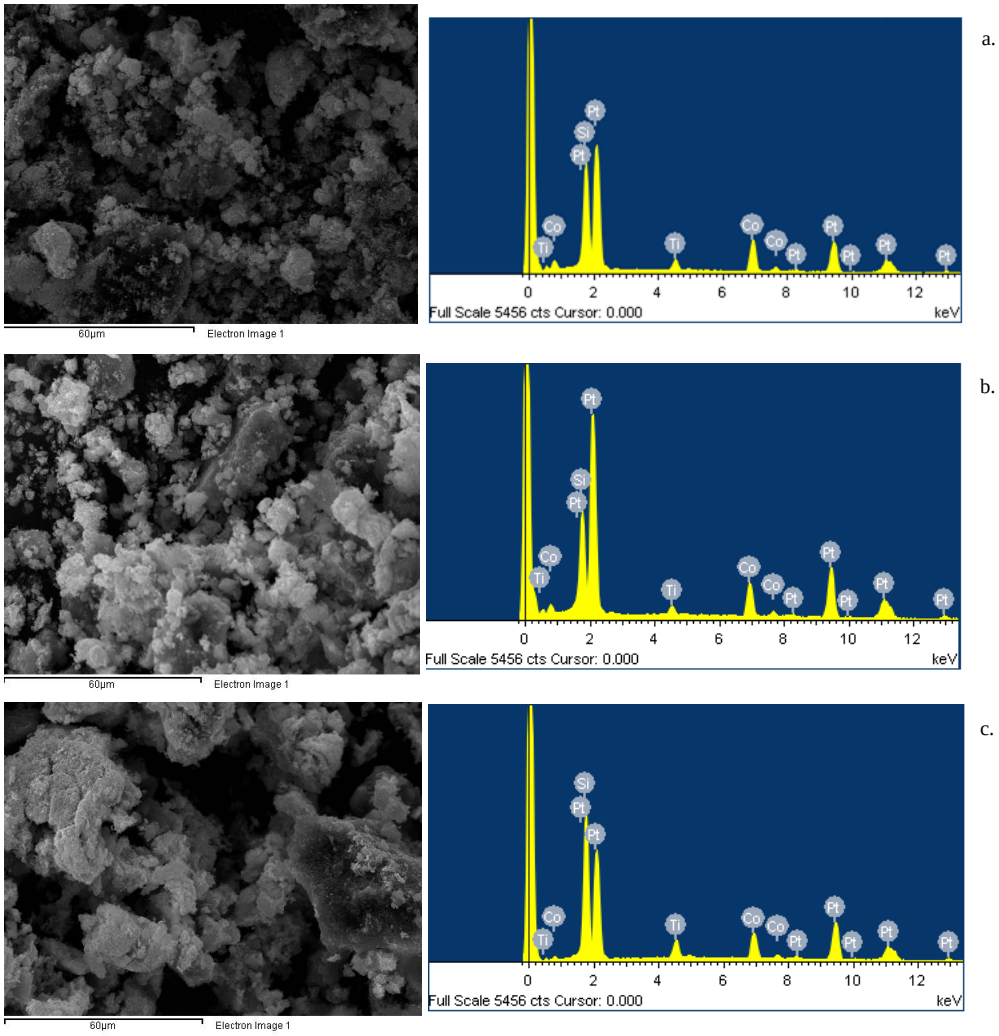

205

206 **Figure 1**. EDX-SEM spectra of PtCo (1:1)/SiCTiC catalysts that were prepared using

207 different synthesis temperatures: a) 30 °C, b) 50 °C and c) 80 °C.

208 The temperature has a strong influence on the dispersion of the metallic particles. As

209 the temperature increases, the agglomeration of the metallic particles increases, which is

210 most likely due to a faster reduction reaction at high temperatures. Therefore, optimal

211 distribution of the PtCo particles is prevented. Figure 2 shows the XRD patterns of Pt and

212 PtCo on SiCTiC and the support. First, the platinum catalyst was successfully deposited

213 on the support because the main peaks corresponding to the platinum crystals were

214 observed. The Pt peaks located at 40°, 47°, 68° and 82° correspond to the (111), (200),

215 (220) and (311) planes, respectively, of face-centered cubic (fcc) Pt. Based on a

comparison of the XRD patterns for Pt/SiCTiC and PtCo/SiCTiC, the peaks shifted to higher angle values when Co was added[40]. Figure 3 shows the XRD patterns of PtCo/SiCTiC prepared at different synthesis temperatures. No obvious peaks that correspond to the presence of free Co or Co and Pt oxides were observed in the XRD patterns. Based on the results in Figures 2 and 3, the particle size was evaluated using the Scherrer equation[41-42], and the alloy degree was evaluated using the Vegard law[40, 43]. First, Bragg's law along with the Pt lattice geometry and the Miller indices (equation (1)) to calculate the lattice parameters.

$$a\ (200) = \frac{\lambda_{k\alpha}}{\sin \theta_{max}} \qquad (1)$$

where $a_{(200)}$ is the lattice parameter for the PtCo alloy corresponding to the (200) peak, $\lambda_{k\alpha}$ is the wavelength of Cu Kα radiation ($\lambda_{k\alpha}$ = 0.15418 nm) and θ_{max} is the angle corresponding to the maximum intensity of the (200) Pt peak.

The cobalt atomic fraction in the alloy and the alloying degree parameters were calculated from equations (2) and (3):

$$a_{PtCo} = a_{Pt} - k \cdot x_{Co} \qquad (2)$$

$$\text{Alloying degree} = \frac{x_{Co}}{[(1 - x_{Co}) \cdot (Co/Pt)_{real}]} \qquad (3)$$

where a_i are the lattices parameters corresponding to Pt and the PtCo alloy, k is the copper constant (k=0.124 Å), x_{Co} is the cobalt atomic fraction and $(Co/Pt)_{real}$ is the real atomic ratio.

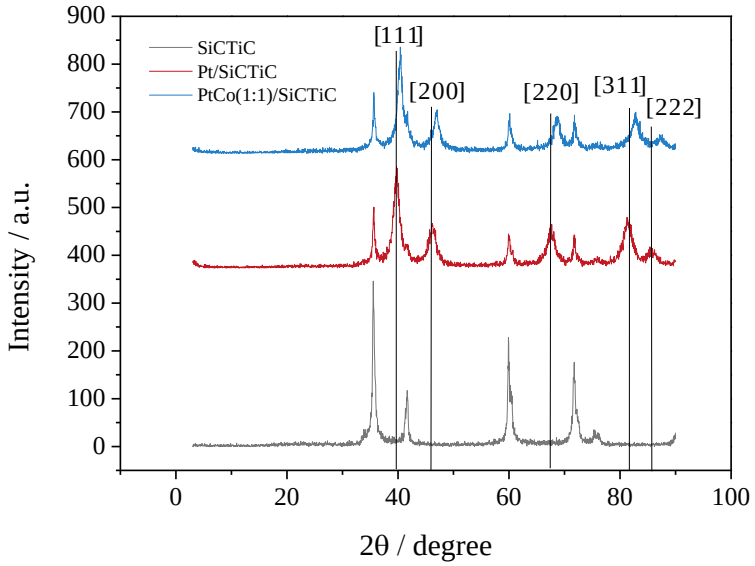

Figure 2. XRD patterns for the support and the Pt/SiCTiC and PtCo/SiCTiC catalysts.

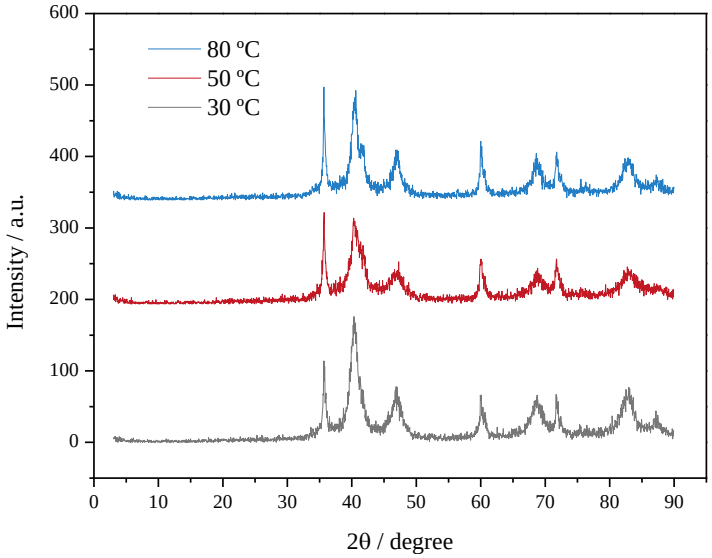

Figure 3. XRD patterns for the PtCo/SiCTiC catalysts that were prepared using different synthesis temperatures.

Table 2 shows the crystal and particle sizes, which were obtained from the XRD patterns and TEM images, respectively, as well as the lattice parameters and alloy degrees of each sample. The obtained crystallite sizes of PtCo/SiCTiC were smaller than those of

245 the Pt/SiCTiC catalyst synthesized using the same method at 80 °C (7.08 nm) and the
246 formic acid method at 80 °C (7.67 nm[19]). A substantial effect of the temperature on the
247 crystal size was observed. As the synthesis temperature increased, the crystallite size
248 increased, which may be due to enhanced reduction efficiency of the Pt precursor salt
249 during the synthesis process due to the higher temperature. This effect may also increase
250 the agglomeration of the metallic particles on the SiCTiC surface due to the low BET area
251 of this material compared to that of carbon black (BET_{SiCTiC} = 99.5 m^2 g^{-1} and
252 $BET_{VulcanXC72}$ = 268 m^2 g^{-1} [19]).

253 Moreover, the addition of smaller cobalt atoms into the Pt lattice resulted in a
254 reduction in the Pt-Pt bond distance, which contracted the crystallite net of the Pt particles
255 due to generation of a PtCo alloy[44-45]. The obtained lattice parameters differ from lattice
256 parameter of pure Pt (a_{Pt} = 0.391 nm) due to the solubility of Co in the face-centered cubic
257 Pt lattice[46]. Taking into account the different atomic sizes (R_{Pt} = 0.139 nm and R_{Co} = 0.125
258 nm), the inclusion of the smaller atoms results in contraction of the Pt crystallite net,
259 which changes the alloy lattice parameter compared to that of Pt[47]. Furthermore, smaller
260 lattice parameters correspond to high alloying degrees[44], which is consistent with the
261 obtained result. The shorter Pt-Pt nearest-neighbor distance in the alloys compared to that
262 of pure Pt results in easier oxygen reduction and enhanced kinetics, increasing the overall
263 fuel cell performance[46]. The influence of the temperature on the synthesis results in two
264 different effects. Therefore, an increase in the temperature increases the alloying degree
265 but results in a larger crystal size.

266 Figure 4 shows the TEM images of the PtCo/SiCTiC powders synthesized at two
267 different temperatures and of the PtCo/Vulcan powder synthesized at 80 ºC. For all
268 catalysts, the PtCo particles were uniformly dispersed over the entire non-carbonaceous
269 support. However, some agglomeration was observed due to the high content of metal

deposited on the support and the low BET surface of SiCTiC (≈100 m^2 g^{-1}) compared to those of others carbonaceous supports, such as Vulcan carbon (250 m^2 g^{-1}). The particle size distributions of the PtCo catalysts were measured for more than 200 particles in each sample. The obtained values were slightly higher than those obtained from XRD data.

Table 2. Crystal sizes and alloying degrees.

Sample	Crystal size XRD (nm)	Particle size TEM (nm)	Lattice parameter	X_{Co}	Alloying degree (%)
PtCo/SiCTiC 30 °C	5.0 ± 0.6	5.6	0.3876	0.27	17.6
PtCo/SiCTiC 50 °C	5.2 ± 1.1	-	0.3867	0.35	27.5
PtCo/SiCTiC 80 °C	6.3 ± 1.5	7.1	0.3864	0.37	29.3
PtCo/Vulcan 80 °C	6.2 ± 0.7	7.5	0.3861	0.39	33.1

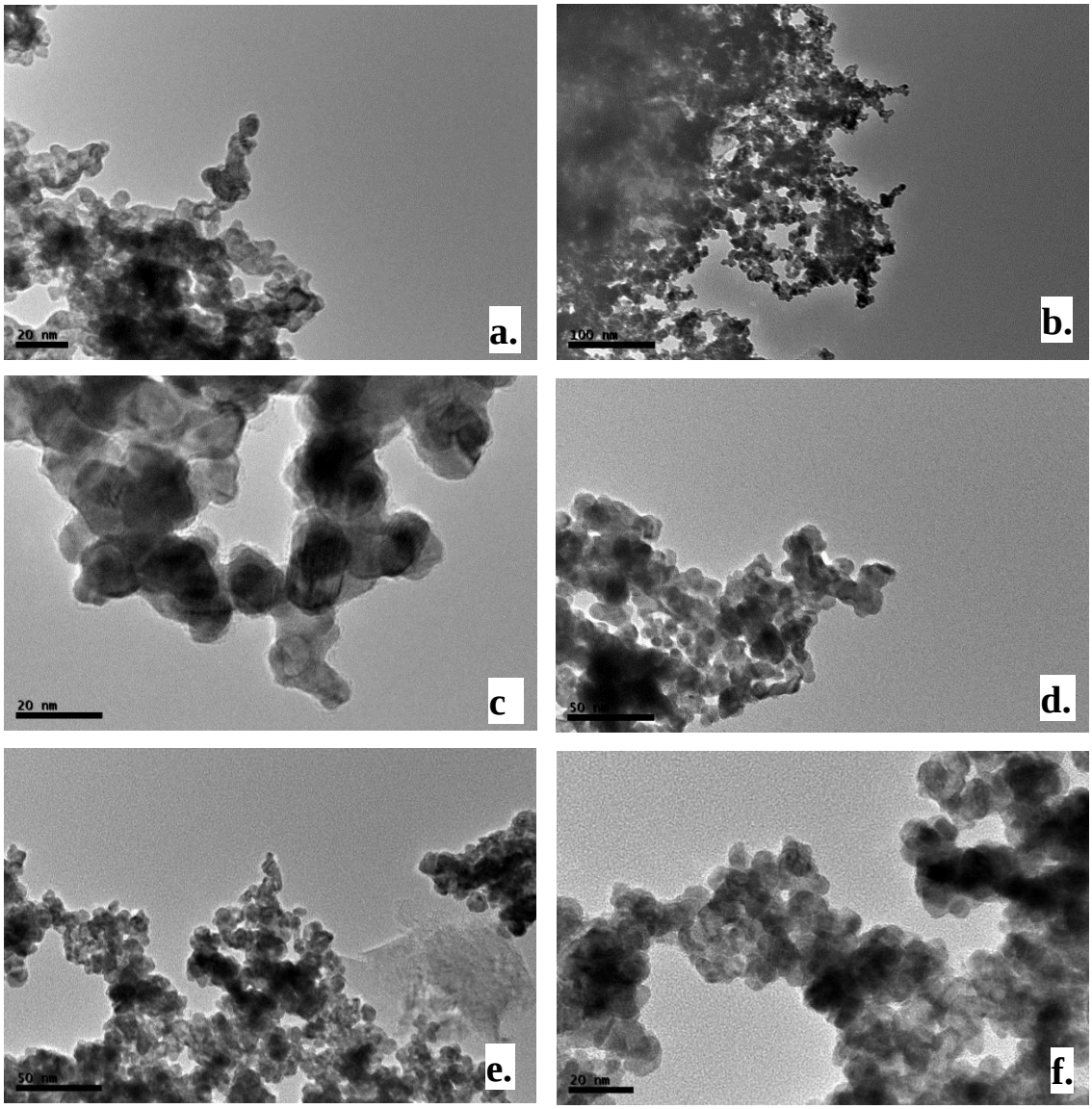

Figure 4. TEM images at different magnifications for the PtCo/SiCTiC catalysts synthesized at 30 °C (a, b) and 80 °C (c, d) and for the PtCo/Vulcan catalyst synthesized at 80 °C (e,f).

3.2. Electrochemical characterization using an RDE

The rotating disk electrode (RDE) technique has been extensively used as a screening tool to estimate the activity of lab-scale (mg) quantities of novel PEMFC electrocatalysts[48].

ECSA was evaluated by integrating the hydrogen adsorption-desorption regions in the CV curves using equation 1:

$$ECSA = \frac{A}{v \cdot C} \cdot \frac{1}{Le} \qquad (1)$$

where *A* is the peak area (AV cm^{-2}), *v* is the scan rate (V s^{-1}), *C* is the charge required to reduce the proton monolayer of the active platinum (0.21 mC cm^{-2}) and *Le* is the platinum load in the catalysts (0.016 and 0.3 mg cm^{-2} for the RDE and electrode, respectively).

Figure 5 shows the voltammograms of PtCo (1:1) / SiCTiC prepared using different synthesis temperatures. The adsorption and desorption regions typically contain two peaks, which are related to the (100) and (111) crystal face planes of Pt[19]. Occasionally, both peaks overlap generating a single peak that corresponds to the more active one, which is the (100) crystal face due to its higher activity[24]. The ECSA values were obtained from cycle 10 to determine the value after stabilization of the system. During the first cycles, the H_2 desorption peak area increased due to hydration of the Nafion ionomer, which was used as a binder, by the electrolyte, which improves the three-phase boundary. However, larger amounts of Nafion may exert a negative effect on the calculation of the ECSA because the close interaction between Pt and Nafion may affect to the H_2 absorption-desorption processes. After the total saturation of the Nafion ionomer with the electrolyte, the ECSA began to decrease due to both the Pt-Nafion interactions and the electrochemical degradation of the catalyst, which was caused by the electrochemical test[24]. The ECSA values were 9.91 and 13.47 $m^2\ g_{Pt}^{-1}$ for the 30 °C and 80 °C synthesized catalysts, respectively. The catalyst synthesized at 50 °C exhibited a very small desorption peak, and the ECSA value could not be calculated. The obtained ECSA values were lower than that of the catalyst without Co ($ECSA_{Pt/SiCTiC}$ = 18.13 $m^2\ g_{Pt}^{-1}$). Yang et al.[49] obtained ECSA values of 20 $m^2\ g_{Pt}^{-1}$ for a Pt catalyst on a novel TiC

support. The higher ECSA values obtained by Yang et al. may be due to its smaller particle size (2.2 nm). However, ECSA values of approximately 4-6 $m^2 g_{Pt}^{-1}$ were also reported for Pt/TiC, which was obtained using different synthesis methods. These values are much lower than the one reported in this study. The high ECSA values are directly related to the availability of the active centers on the electrocatalysts. Therefore, a higher synthesis temperature results in a PtCo catalyst with enhanced activity, which is most likely due to high efficiency during reduction of the metallic precursors[20].

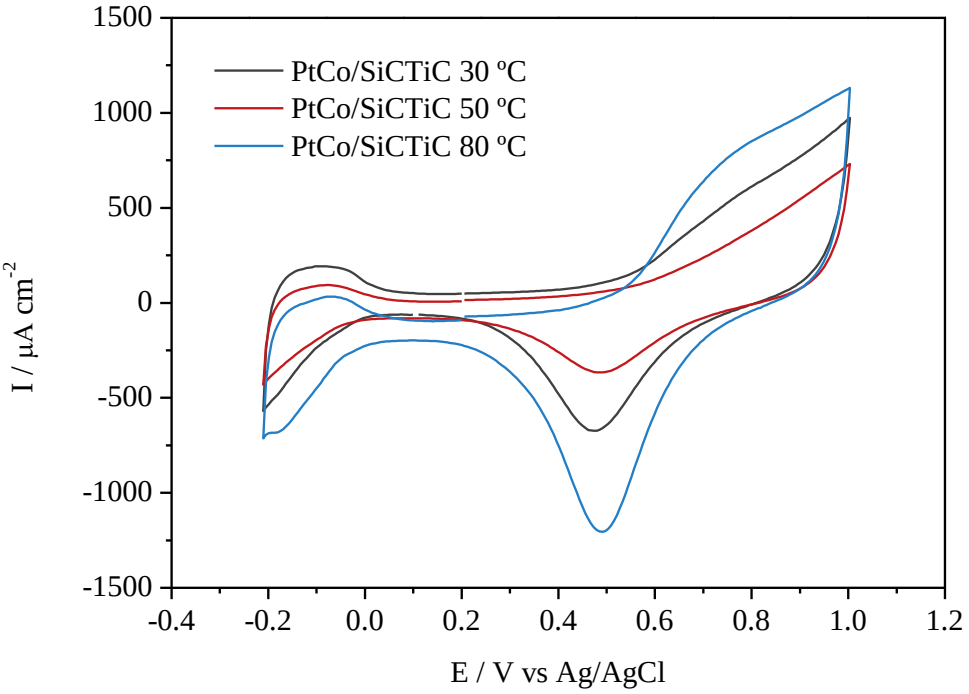

Figure 5. Cyclic voltammetry curves for PtCo (1:1) / SiCTiC prepared using different synthesis temperatures, which were recorded at room temperature in N_2-purged 0.5 M H_2SO_4 solutions at a sweep rate of 50 mV s^{-1}.

The observed electrochemical surface area decreased with the addition of a second metal since the presence of cobalt oxide could increase the contribution to the double layer, which would decrease the observed H_2 desorption peak region. Furthermore, the cobalt oxide could block the Pt active centers, which would decrease the electrochemical active area of the PtCo-based catalyst [40,50]. The increase in the current density in the high

potential region may be due to oxygen evolution, which decreased resulting from the presence of more oxides due to the cobalt species. To confirm this hypothesis, TPR analyses of the catalysts PtCo/SiCTiC synthesized at different temperatures were performed. Figure 6 shows the TPR profiles for all the synthesized catalysts. The H_2 adsorption peaks were 154, 198 and 130 µmol g_{H2}^{-1} for the catalysts synthesized at 30, 50 and 80 °C, respectively. The sample synthesized at 50 °C exhibited the highest H_2 adsorption area, which indicates the highest oxide content. This result explains this sample possessing the lowest ECSA value, as shown in Figure 5. Based on comparison of these results to the Co and Pt wt%, the catalyst synthesized at 80 °C possessed a lower ECSA due to the higher Co content in the catalyst. In addition, a large crystal size and low dispersion decreased the active area of the catalyst[44], which explains the obtained results.

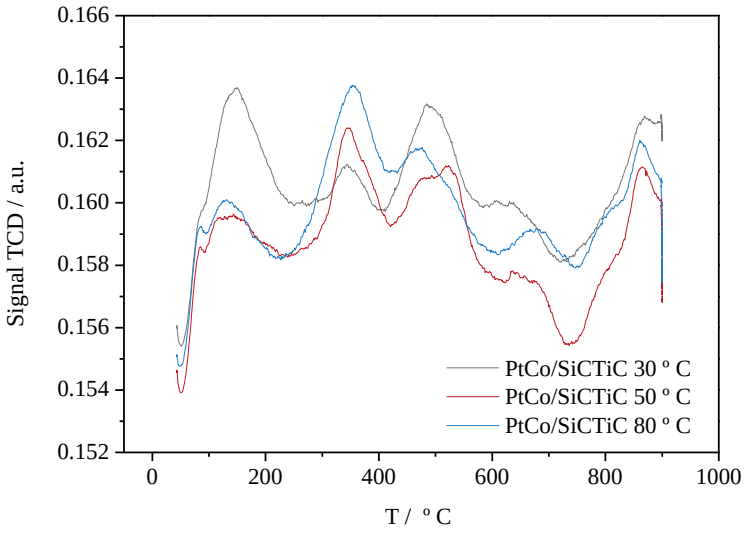

Figure 6. TPR profile of the different catalysts prepared under flowing gas consisting of 5 vol.% H_2/Ar. Heating rate: 5 °C min^{-1}.

Figure 7 shows the evolution of the mass activity as a function of time for the different catalysts at 0.55 V, and the experiment was performed at room temperature in 0.5 M H_2SO_4 saturated in O_2. Table 3 shows the percent degradation suffered by the different catalysts. The PtCo/SiCTiC samples demonstrated lower currents than Pt alone. However, the PtCo-based catalysts exhibited higher stability than the pure Pt catalysts in terms of current density drops, which indicates that the presence of the non-precious metal may prevent migration of the platinum particles on the support[4, 28]. Moreover, when the SiCTiC and Vulcan XC72 supports were compared, the carbonaceous-supported catalysts exhibited more degradation than the non-carbonaceous one, as expected. Furthermore, the PtCo alloys with large particle sizes (synthesized at higher temperatures) were more stable[51-52].

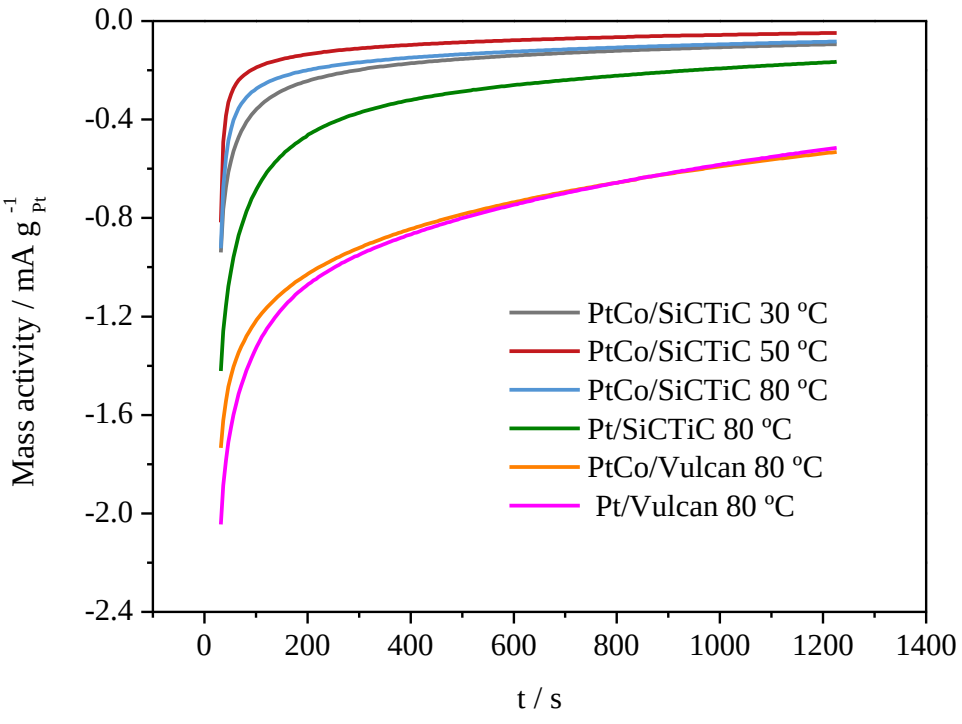

Figure 7. Chronoamperometric results for different catalysts at 0.55 V in 0.5 M H_2SO_4 (rotation disk electrode, ω= 1000 rpm).

Table 3. Degradation after chronoamperometric analysis

Catalyst	Degradation / mA g_{Pt}^{-1} s^{-1}
PtCo/SiCTiC 30 °C	7.382E-5
PtCo/SiCTiC 50 °C	4.790E-5
PtCo/SiCTiC 80 °C	6.534E-5
Pt/SiCTiC 80 °C	1.508E-4
PtCo/Vulcan 80 °C	3.278E-4
Pt/Vulcan 80 °C	3.701E-4

356

357 The oxygen reduction reactions were performed to evaluate the catalytic activity
358 using the Tafel plot and the electron transfer number from the Koutecky-Levich equation.
359 Table 4 shows the Tafel values and the limiting current density values at different rotation
360 rates and temperatures. Tafel slopes of 60 mV dec^{-1} correspond to an oxygen reduction
361 mechanism that involves an initial fast charge transfer step followed by a chemical step,
362 which is determined under Langmuir conditions[53-54]. The result indicates Tafel values
363 higher than 60 mV dec^{-1}, which may be result from a low O_2 concentration in the
364 background due to a mixed activation/mass transport control[55]. Liu et al.[6] obtained Tafel
365 plot values in H_3PO_4 of the same order of magnitude (98 mV dec^{-1}) as the results obtained
366 in the current study. The results do not show any relationship between the kinetic reaction
367 and the synthesis temperature. However, an increase in the kinetic reaction and limit
368 current density was observed as a function of the rotation rate due to the increase in the
369 rotation rate decreasing the mass transfer resistance. The low activity of the ORR in the
370 PtCo/SiCTiC catalyst synthesized at 80 °C may be related to the oxide content on the
371 catalyst surface. It is important to note that the lower H_2 adsorption areas may explain the
372 higher ORR activity achieved by the catalysts synthesized at 30 and 80 °C because the
373 oxide content on the catalyst surface was lower than that on the catalyst synthesized at 50
374 °C. Low crystal sizes increase the metallic surface exposed to the media, which increases
375 the oxide formation, blocks the active site for oxygen adsorption and decreases the ORR
376 activity. Furthermore, as previously mentioned, the lower synthesis temperature may

prevent complete metallic reduction, which is consistent with the lower alloying degree, and decrease the catalytic activity of the resulting PtCo catalyst[56].

Table 4. Tafel slope and limit current density at different rotation rates.

	Tafel slope (mV dec^{-1})			Limiting current density (A cm^{-2})		
t^a (ºC) / ω (rpm)	30 ºC	50 ºC	80 ºC	30 ºC	50 ºC	80 ºC
400	88.5	124.9	109.4	0.00166	0.00195	0.00235
800	86.9	122.3	108.3	0.00214	0.0027	0.00319
1200	84.6	121.4	106.5	0.00243	0.00299	0.00384
1600	82.2	121.1	106	0.00262	0.00332	0.00435

Figure 8 shows the Koutecky-Levich plot for the synthesized catalysts. The parallelism and linearity observed in this plot indicates first order kinetics with respect to molecular oxygen[57-58]. Based on these results, the transferred electron number in the oxygen reduction reaction was calculated to be 3.18, 3.30 and 3.58 for the PtCo/SiCTiC catalysts synthesized at 30, 50 and 80 °C, respectively. A lower n value may indicate the production of H_2O_2. This fact may be related to the presence of oxides on the catalytic surface and the Co oxide presence, which may cause non-complete reduction of the oxygen to H_2O[39]. Moreover, these values are higher than other previously reported values for PtCo-based catalysts. Hyun K. et al. obtained *n* values of approximately 2.8 for PtCo/C catalysts prepared using the same method[40], which is smaller than the results for these catalysts.

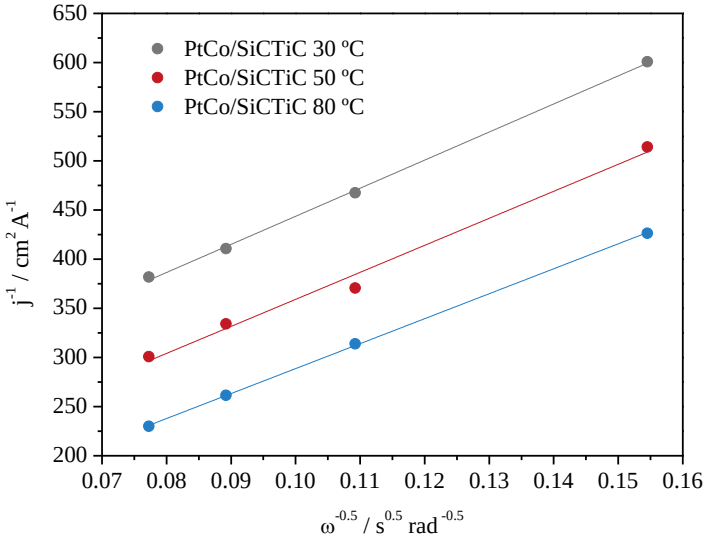

391

392 **Figure 8.** Plot of 1/j as a function of $1/\sqrt{\omega}$ from the experimental data for H_2O_2

393 reduction on Pt in 0.5 M H_2SO_4 at 25 °C.

394 **3.3. Electrochemical characterization using a half-cell**

395 To achieve complete ex situ characterization after the RDE evaluation, electrodes
396 were prepared using the catalysts, and electrochemical activity was exhibited (catalysts
397 synthesized at 30 °C and 80 °C) in the half-cell test. The ECSA and its loss was evaluated
398 in a H_3PO_4 medium, which was closer to the fuel cell conditions.

399 Figure 9 shows the evolution of the voltammograms of the PtCo/Vulcan catalysts
400 synthesized at 80 °C and the PtCo/SiCTiC catalysts synthesized at 30 and 80 °C. The
401 measurements were recorded at 50 °C in N_2-purged 2 M H_3PO_4 solutions at a sweep rate
402 of 50 mV s^{-1}. The oxidation of the carbon surface on carbon black in aqueous acid
403 electrolytes occurs at a potential close to 0.6 V (vs. RHE)[4, 59]. In this case, the steep
404 hydroquinone-quinone (HQ-Q) peak at approximately 0.4 V (vs Ag/AgCl) that was
405 observed in the PtCo/Vulcan CV curve after 400 cycles indicated surface oxidation. This
406 difference between the carbonaceous and non-carbonaceous supports confirms the poorer

degree of electrochemical stability of the carbonaceous supports[38, 60]. In contrast to the cyclic voltammetry curves of the PtCo/SiCTiC catalysts in the RDE, the half-cell CV curves display more differentiated (100) and (111) Pt crystal faces. However, an overlap continues to be observed. Both peaks are observed in the adsorption and desorption regions. The obtained ECSA values of the PtCo/SiCTiC catalysts synthesized at 30 and 80 °C were 10.6 and 11.3 $m^2 g_{Pt}^{-1}$, respectively. The higher double layer contribution for the PtCo/SiCTiC catalyst synthesized at 30 °C can mask a portion of the H_2 absorption/desorption peak, reducing the observed active area[61]. Double layer changes were not shown after 400 cycles, which indicates that these materials do not exhibit important structural or chemical changes during the experiments. Moreover, a higher electrochemical stability was observed for the PtCo/SiCTiC catalyst synthesized at 80 ° C (17% ECSA loss compared to 21% ECSA loss for the PtCo/SiCTiC catalyst synthesized at 30°C). The larger crystallite size of this catalyst may improve the electrochemical resistance of the catalyst, which may prevent agglomeration and catalyst migration processes. Furthermore, the higher alloying degree reached by the catalyst prepared at the highest temperature may be beneficial for achieving higher stability. The ECSA losses may be due to polarization of the catalysts in acid media and corrosion of the carbon support[24]. In a previous study, the electrochemical activity of the Pt/SiCTiC catalysts was evaluated, and an ECSA value of 7.93 $m^2 g_{Pt}^{-1}$ was reported[19]. Although the addition of a second metal could decrease the ECSA, the crystal size reduction due to formation of the PtCo alloy increases the availability of active centers for oxygen adsorption, which results in an increase in the ECSA[53].

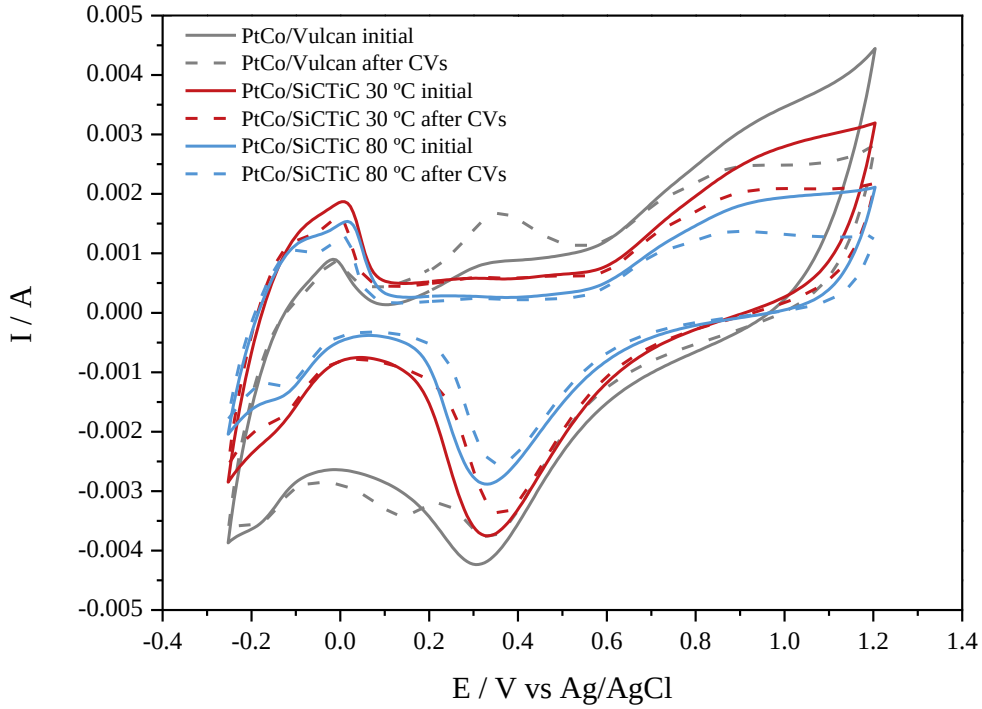

Figure 9. Cyclic voltammograms of different catalysts recorded at 50 °C in N_2-purged 2 M H_3PO_4 solutions at a sweep rate of 50 mV s^{-1}.

3.4. Tests in a single HT-PEMFC

Finally, taking into account that this technology is close to entering the market, the novel prepared and characterized materials were tested in a single fuel cell operating at 160 °C to gain insight into the performance of the PtCo-based catalyst in a real HT-PEMFC system. The best bimetallic catalyst based on the ex situ characterization (PtCo/SiCTiC synthesized at 80 °C) and a PtCo/Vulcan catalyst were used as a cathode catalyst to prepare an MEA according to the procedure described in section 2.4, and this system was tested according to the conditions described in section 2.5.3. Figures 10A and 10B show the polarization curves recorded at different times with oxygen and air, respectively. The evolution of the voltage as a function of time at a constant j of 0.3 A cm^{-2} for the evaluated MEA and other MEA prepared with Vulcan as the catalyst support is shown in Figure 10C.

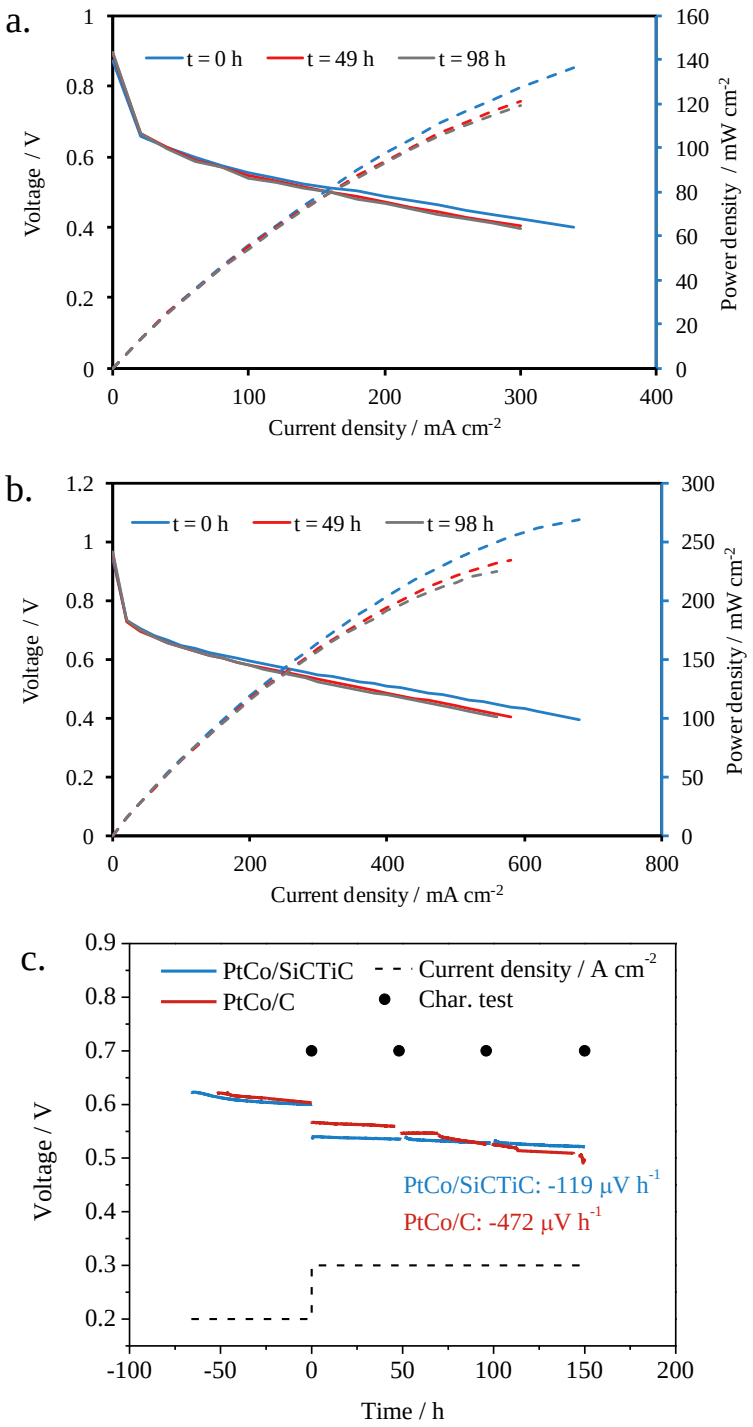

446

447 **Figure 10.** Polarization curves as a function of time with (a) air and (b) oxygen. (c)

448 Evolution of the fuel cell voltage as a function of time at a constant load for the MEAs

449 prepared with PtCo/SiCTiC and PtCo/Vulcan catalysts on the cathode side. Black points

450 indicate the time at which the polarization curves were recorded.

As shown in Figure 10C, both PtCo-based catalysts exhibit similar potential values during the first 100 hours of the preliminary short test. However, PtCo/SiCTiC exhibits much better stability (-119 µV/h vs -472 µV/h reached by the carbonaceous-based catalyst), which indicates that the SiCTiC support avoids degradation of the metallic electrocatalyst particles better than Vulcan carbon XC72. Regarding the polarization curves, the obtained values are closer to the other values found in the literature for PtCo-based catalysts in smaller HT-PEMFC systems[62]. Table 5 compares the power density per mg Pt and the voltages achieved by the PtCo-based MEAs after a 48 hour test. By comparing to the same parameters obtained for a standard Pt/C MEA under the same conditions[61], the ECSA and ORR activity during the ex situ characterization were slightly lower than the Pt-based catalysts. Both PtCo-based MEAs exhibited slightly higher power density values (8% lower than PtCo/SiCTiC and 4% lower than PtCo/C-based MEAs, respectively) per mg of Pt. However, the performance in terms of the voltage was lower (i.e., approximately 30 mV lower than that for the Pt/C-based MEA, as expected from the real Pt loading being lower, and the bimetallic catalyst manufacturing method is not fully optimized, which indicates that this values could be improved. Figure 11 shows TEM images at different magnifications for PtCo/Vulcan and PtCo/SiCTiC electrodes after electrochemical tests. The particles size were calculated to evaluate their change. The PtCo/Vulcan particles size increased from 7.5 to 15.1 nm (100 %) and from 7.1 to 12.4 nm (75 %) for the PtCo/SiCTiC catalyst. These results mean that the alloy supported on non-carbonaceous support suffered of a lower agglomeration effect. On the other hand, it can be also observed, in Figure 11, how in the case of the PtCo on Vulcan samples some areas are empty whereas other areas show high agglomeration (dark black zones in Figure 11.b). This could be explained by the Ostwald ripening which is a well-known degradation mechanism of catalyst of electrodes of PEMFCs [63, 64].

476 **Table 5.** Comparison between the voltage and power density values at same current

477 densities for different MEAs.

	PtCo (2:1)/SiCTiC		40% Pt/Vulcan commercial		40% PtCo (2:1)/Vulcan	
Current density (mA cm^{-2})	Voltage (V)	Power density (W cm^{-2} mg^{-1} Pt)	Voltage (V)	Power density (W cm^{-2} mg^{-1} Pt)	Voltage (V)	Power density (W cm^{-2} mg^{-1} Pt)
100	0.64	0.124	0.684	0.114	0.631	0.119
200	0.58	0.223	0.619	0.206	0.561	0.213

478

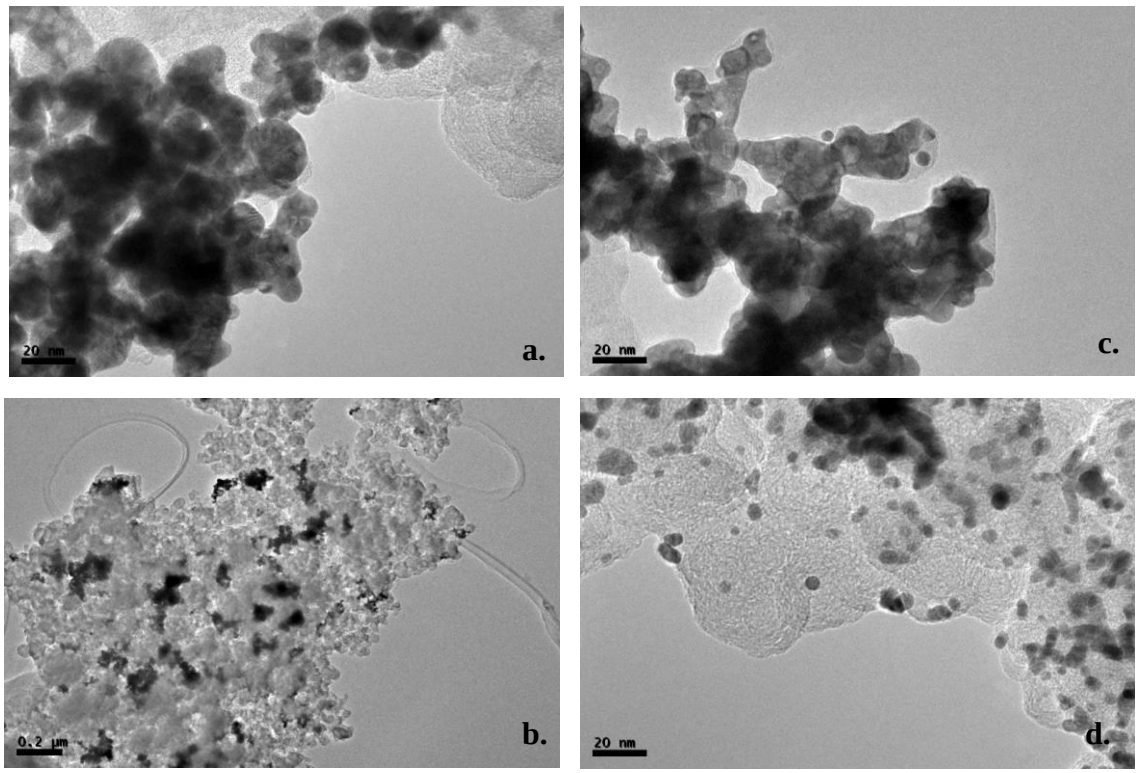

479

480 **Figure 11.** TEM images at different magnifications for PtCo/Vulcan catalyst (a,b) and

481 PtCo/SiCTiC catalyst (c,d).

4. Conclusions

Considering our results, the main conclusions are as follows:

- PtCo-based catalysts on a novel SiCTiC support were successfully synthesized. The support has a strong influence on the final properties of the catalysts, especially in terms of stability.
- Temperature affects the properties of the PtCo/SiCTiC catalysts, and the best results in terms of durability and performance were obtained with the PtCo catalysts synthesized at 80 °C, which was most likely due to the higher alloying degree.
- The PtCo nanocatalyst exhibited a slightly better performance per mg of Pt than the pure Pt-based catalysts under the same operation conditions. In addition, the PtCo/SiCTiC catalyst exhibited promising performance and stability for use in HT-PEMFC technology. Further studies must be performed to optimize the synthesis method and electrode composition to increase the performance of this novel catalyst.

Acknowledgements

The authors wish to thank the University of Castilla-La Mancha for the pre-doctoral fellowship (Grant BIN1630) awarded to María Millán.

References

1. Habibi, B.; Ghaderi, S., Synthesis, Characterization and Electrocatalytic Activity of Co@Pt Nanoparticles Supported on Carbon-Ceramic Substrate for Fuel Cell Applications. *Int. J. Hydrogen Energy* **2015,** *40* (15), 5115-5125.
2. Chen, D.; Zhao, Y.; Fan, Y.; Wang, W.; Li, X.; Peng, X.; Wang, X.; Tian, J., Preparation and Characterization of Core–Shell-Like PbPt Nanoparticles Electro-Catalyst Supported on Graphene for Methanol Oxidation. *Int. J. Hydrogen Energy* **2014,** *39* (28), 16053-16060.
3. Zhang, J.; Byeon, A.; Lee, J. W., Boron-Doped Carbon-iron Nanocomposites as Efficient Oxygen Reduction Electrocatalysts Derived from Carbon Dioxide. *Chem. Commun.* **2014,** *50* (48), 6349-6352.

4. Borup, R.; Meyers, J.; Pivovar, B.; Kim, Y. S.; Mukundan, R.; Garland, N.; Myers, D.; Wilson, M.; Garzon, F.; Wood, D.; Zelenay, P.; More, K.; Stroh, K.; Zawodzinski, T.; Boncella, J.; McGrath, J. E.; Inaba, M.; Miyatake, K.; Hori, M.; Ota, K.; Ogumi, Z.; Miyata, S.; Nishikata, A.; Siroma, Z.; Uchimoto, Y.; Yasuda, K.; Kimijima, K.-i.; Iwashita, N., Scientific Aspects of Polymer Electrolyte Fuel Cell Durability and Degradation. *Chem. Rev.* **2007,** *107* (10), 3904-3951.
5. Liu, Z.; Wainright, J. S.; Savinell, R. F., High-Temperature Polymer Electrolytes for PEM Fuel Cells: Study of the Oxygen Reduction Reaction (ORR) at a Pt–Polymer Electrolyte Interface. *Chem. Eng. Sci.* **2004,** *59* (22–23), 4833-4838.
6. Liu, Z.; Wainright, J. S.; Litt, M. H.; Savinell, R. F., Study of the Oxygen Reduction Reaction (ORR) at Pt Interfaced with Phosphoric Acid Doped Polybenzimidazole at Elevated Temperature and Low Relative Humidity. *Electrochim. Acta* **2006,** *51* (19), 3914-3923.
7. Zeis, R., Materials and Characterization Techniques for High-Temperature Polymer Electrolyte Membrane Fuel Cells. *Beilstein J. Nanotechnol.* **2015,** *6*, 68-83.
8. Lobato, J.; Cañizares, P.; Rodrigo, M. A.; Úbeda, D.; Pinar, F. J., A Novel Titanium PBI-Based Composite Membrane for High Temperature PEMFCs. *J. Membr. Sci.* **2011,** *369* (1–2), 105-111.
9. Okamoto, M.; Fujigaya, T.; Nakashima, N., Design of an Assembly of Poly(benzimidazole), Carbon Nanotubes, and Pt Nanoparticles for a Fuel-Cell Electrocatalyst with an Ideal Interfacial Nanostructure. *Small* **2009,** *5* (6), 735-740.
10. Sharma, S.; Pollet, B. G., Support Materials for PEMFC and DMFC Electrocatalysts—A Review. *J. Power Sources* **2012,** *208*, 96-119.
11. d'Arbigny, J. B.; Taillades, G.; Marrony, M.; Jones, D. J.; Roziere, J., Hollow Microspheres with a Tungsten Carbide Kernel for PEMFC Application. *Chem. Commun.* **2011,** *47* (28), 7950-7952.
12. Avasarala, B.; Murray, T.; Li, W.; Haldar, P., Titanium Nitride Nanoparticles Based Electrocatalysts for Proton Exchange Membrane Fuel Cells. *J. Mater. Chem.* **2009,** *19* (13), 1803-1805.
13. Yin, S.; Mu, S.; Lv, H.; Cheng, N.; Pan, M.; Fu, Z., A Highly Stable Catalyst for PEM Fuel Cell Based on Durable Titanium Diboride Support and Polymer Stabilization. *Appl. Catal., B* **2010,** *93* (3–4), 233-240.
14. Huang, S.-Y.; Ganesan, P.; Park, S.; Popov, B. N., Development of a Titanium Dioxide-Supported Platinum Catalyst with Ultrahigh Stability for Polymer Electrolyte Membrane Fuel Cell Applications. *J. Am. Chem. Soc.* **2009,** *131* (39), 13898-13899.
15. Lv, H.; Mu, S.; Cheng, N.; Pan, M., Nano-Silicon Carbide Supported Catalysts for PEM Fuel Cells with High Electrochemical Stability and Improved Performance by Addition of Carbon. *Appl. Catal., B* **2010,** *100* (1–2), 190-196.
16. Dong, L.; Tong, X.; Wang, Y.; Guo, X.; Jin, G.; Guo, X., Promoting Performance and CO Tolerance of Pt Nanocatalyst for Direct Methanol Fuel Cells by Supporting on High-Surface-Area Silicon Carbide. *J. Solid State Electrochem.* **2013,** *18* (4), 929-934.
17. Deneuve, A.; Florea, I.; Ersen, O.; Nguyen, P.; Pham, C.; Bégin, D.; Edouard, D.; Ledoux, M.-J.; Pham-Huu, C., Catalytic Growth of Silicon Carbide Composite with Nanoscopic Properties and Enhanced Oxidative Resistance as Catalyst Support. *Appl. Catal., A* **2010,** *385* (1–2), 52-61.
18. Dhiman, R.; Stamatin, S. N.; Andersen, S. M.; Morgen, P.; Skou, E. M., Oxygen Reduction and Methanol Oxidation Behaviour of SiC Based Pt Nanocatalysts for Proton Exchange Membrane Fuel Cells. *J. Mater. Chem. A* **2013,** *1* (48), 15509-15516.
19. Lobato, J.; Zamora, H.; Plaza, J.; Rodrigo, M. A., Composite Titanium Silicon Carbide as a Promising Catalyst Support for High-Temperature Proton-Exchange Membrane Fuel Cell Electrodes. *ChemCatChem* **2016,** *8* (4), 848-854.
20. Yang, T.; Ma, Y.; Huang, Q.; Cao, G., Palladium–Iridium Nanocrystals for Enhancement of Electrocatalytic Activity toward Oxygen Reduction Reaction. *Nano Energy* **2016,** *19*, 257-268.

21. Shrestha, S.; Ashegi, S.; Timbro, J.; Lang, C. M.; Mustain, W. E., ORR and Fuel Cell Performance of Pt Supported on N-Functionalized Mesoporous Carbon. *ECS Trans.* **2011,** *41* (1), 1183-1191.
22. Okada, Y.; Ishihara, A.; Matsumoto, M.; Arao, M.; Imai, H.; Kohno, Y.; Matsuzawa, K.; Mitsushima, S.; Ota, K., Effect of Reheating Treatment on Oxygen-Reduction Activity and Stability of Zirconium Oxide-Based Electrocatalysts Prepared from Oxy-Zirconium Phthalocyanine for Polymer Electrolyte Fuel Cells. *J. Electrochem. Soc.* **2015,** *162* (9), F959-F964.
23. Min, M.-k.; Cho, J.; Cho, K.; Kim, H., Particle Size and Alloying Effects of Pt-based Alloy Catalysts for Fuel Cell Applications. *Electrochim. Acta* **2000,** *45* (25–26), 4211-4217.
24. Colón-Mercado, H. R.; Popov, B. N., Stability of Platinum Based Alloy Cathode Catalysts in PEM Fuel Cells. *J. Power Sources* **2006,** *155* (2), 253-263.
25. Liao, H.; Fisher, A.; Xu, Z. J., Surface Segregation in Bimetallic Nanoparticles: A Critical Issue in Electrocatalyst Engineering. *Small* **2015,** *11* (27), 3221-3246.
26. Jalan, V.; Taylor, E. J., Importance of Interatomic Spacing in Catalytic Reduction of Oxygen in Phosphoric Acid. *J. Electrochem. Soc.* **1983,** *130* (11), 2299-2302.
27. Toda, T.; Igarashi, H.; Uchida, H.; Watanabe, M., Enhancement of the Electroreduction of Oxygen on Pt Alloys with Fe, Ni, and Co. *J. Electrochem. Soc.* **1999,** *146* (10), 3750-3756.
28. Antolini, E.; Salgado, J. R. C.; Gonzalez, E. R., The Stability of Pt–M (M = First Row Transition Metal) Alloy Catalysts and its Effect on the Activity in Low Temperature Fuel Cells: A Literature Review and Tests on a Pt–Co Catalyst. *J. Power Sources* **2006,** *160* (2), 957-968.
29. Liang, Y.; Zhang, H.; Yi, B.; Zhang, Z.; Tan, Z., Preparation and Characterization of Multi-Walled Carbon Nanotubes Supported PtRu Catalysts for Proton Exchange Membrane Fuel Cells. *Carbon* **2005,** *43* (15), 3144-3152.
30. Erikson, H.; Sarapuu, A.; Tammeveski, K.; Solla-Gullón, J.; Feliu, J. M., Enhanced Electrocatalytic Activity of Cubic Pd Nanoparticles towards the Oxygen Reduction Reaction in Acid Media. *Electrochem. Commun.* **2011,** *13* (7), 734-737.
31. Chen, Z.; Deng, W.; Wang, X.; Yan, Y., Durability and Activity Study of Single-Walled, Double-Walled and Multi-Walled Carbon Nanotubes Supported Pt Catalyst for PEMFCs. *ECS Trans.* **2007,** *11* (1), 1289-1299.
32. Yano, H.; Watanabe, M.; Iiyama, A.; Uchida, H., Particle-Size Effect of Pt Cathode Catalysts on Durability in Fuel Cells. *Nano Energy* **2016**, 29, 323-333.
33. Lobato, J.; Cañizares, P.; Rodrigo, M. A.; Linares, J. J.; Úbeda, D.; Pinar, F. J., Study of the Catalytic Layer in Polybenzimidazole-based High Temperature PEMFC: Effect of Platinum Content on the Carbon Support. *Fuel Cells* **2010,** *10* (2), 312-319.
34. Pushkarev, A. S.; Pushkareva, I. V.; Grigoriev, S. A.; Kalinichenko, V. N.; Presniakov, M. Y.; Fateev, V. N., Electrocatalytic Layers Modified by Reduced Graphene Oxide for PEM Fuel Cells. *Int. J. Hydrogen Energy* **2015,** *40* (42), 14492-14497.
35. Smirnova, A.; Dong, X.; Hara, H.; Vasiliev, A.; Sammes, N., Novel Carbon Aerogel-Supported Catalysts for PEM Fuel Cell Application. *Int. J. Hydrogen Energy* **2005,** *30* (2), 149-158.
36. Andersen, S. M.; Borghei, M.; Lund, P.; Elina, Y.-R.; Pasanen, A.; Kauppinen, E.; Ruiz, V.; Kauranen, P.; Skou, E. M., Durability of Carbon Nanofiber (CNF) & Carbon Nanotube (CNT) as Catalyst Support for Proton Exchange Membrane Fuel Cells. *Solid State Ionics* **2013,** *231*, 94-101.
37. Lobato, J.; Cañizares, P.; Rodrigo, M. A.; Linares, J. J., PBI-based Polymer Electrolyte Membranes Fuel Cells: Temperature Effects on Cell Performance and Catalyst Stability. *Electrochim. Acta* **2007,** *52* (12), 3910-3920.
38. Lobato, J.; Zamora, H.; Cañizares, P.; Plaza, J.; Rodrigo, M. A., Microporous Layer Based on SiC for High Temperature Proton Exchange Membrane Fuel Cells. *J. Power Sources* **2015,** *288*, 288-295.
39. He, Q.; Mukerjee, S., Electrocatalysis of Oxygen Reduction on Carbon-Supported PtCo Catalysts Prepared by Water-in-Oil Micro-Emulsion. *Electrochim. Acta* **2010,** *55* (5), 1709-1719.

40. Kyuhwan Hyun, J. H. L., Chang Won Yoon and Yongchai Kwon The Effect of Platinum Based Bimetallic Electrocatalysts on Oxygen Reduction Reaction of Proton Exchange Membrane Fuel Cells *Int. J. Electrochem. Sci.* **2013,** *8*, 11752-11767.
41. H. P. Klug, L. E. A., X-ray Diffraction Procedures form Polycrystalline and Amorphous Materials. **1974**, Willey, New York.
42. Leontyev, I. N.; Guterman, V. E.; Pakhomova, E. B.; Timoshenko, P. E.; A.V.Guterman; Zakharchenko, I. N.; Petin, G. P.; Dkhil, B., XRD and Electrochemical Investigation of Particle Size Effects in Platinum-Cobalt Cathode Electrocatalysts for Oxygen Reduction. *J. Alloys Compd.* **2010,** *500* (2), 241-246.
43. Antolini, E.; Cardellini, F., Formation of Carbon Supported PtRu Alloys: an XRD Analysis. *J. Alloys Compd.* **2001,** *315* (1–2), 118-122.
44. Hyun, M.-S.; Kim, S.-K.; Lee, B.; Peck, D.; Shul, Y.; Jung, D., Effect of NaBH4 Concentration on the Characteristics of PtRu/C Catalyst for the Anode of DMFC Prepared by the Impregnation Method. *Catal. Today* **2008,** *132* (1–4), 138-145.
45. Kuttiyiel, K. A.; Choi, Y.; Hwang, S.-M.; Park, G.-G.; Yang, T.-H.; Su, D.; Sasaki, K.; Liu, P.; Adzic, R. R., Enhancement of the Oxygen Reduction on Nitride Stabilized Pt-M (M=Fe, Co, and Ni) Core–Shell Nanoparticle Electrocatalysts. *Nano Energy* **2015,** *13*, 442-449.
46. Rao, C. V.; Parrondo, J.; Ghatty, S. L.; Rambabu, B., High Temperature Polymer Electrolyte Membrane Fuel Cell Performance of PtxCoy/C Cathodes. *J. Power Sources* **2010,** *195* (11), 3425-3430.
47. Lobato, J.; Cañizares, P.; Rodrigo, M. A.; Linares, J. J., Study of Different Bimetallic Anodic Catalysts Supported on Carbon for a High Temperature Polybenzimidazole-Based Direct Ethanol Fuel Cell. *Appl. Catal., B* **2009,** *91* (1–2), 269-274.
48. Shinozaki, K.; Zack, J. W.; Richards, R. M.; Pivovar, B. S.; Kocha, S. S., Oxygen Reduction Reaction Measurements on Platinum Electrocatalysts Utilizing Rotating Disk Electrode Technique: I. Impact of Impurities, Measurement Protocols and Applied Corrections. *J. Electrochem. Soc.* **2015,** *162* (10), F1144-F1158.
49. Yang, L.; Kimmel, Y. C.; Lu, Q.; Chen, J. G., Effect of Pretreatment Atmosphere on the Particle Size and Oxygen Reduction Activity of Low-Loading Platinum Impregnated Titanium Carbide Powder Electrocatalysts. *J. Power Sources* **2015,** *287*, 196-202.
50. Szabó, S.; Bakos, I.; Nagy, F., Investigation of Ruthenium Deposition onto a Platinum Electrode in Hydrochloric Acid Media. *J. Electroanal. Chem. Interfacial Electrochem.* **1989,** *271* (1–2), 269-277.
51. Beard, B. C.; Ross, P. N., Characterization of a Titanium-Promoted Supported Platinum Electrocatalyst. *J. Electrochem. Soc.* **1986,** *133* (9), 1839-1845.
52. Watanabe, M.; Tsurumi, K.; Mizukami, T.; Nakamura, T.; Stonehart, P., Activity and Stability of Ordered and Disordered Co-Pt Alloys for Phosphoric Acid Fuel Cells. *J. Electrochem. Soc.* **1994,** *141* (10), 2659-2668.
53. Thanasilp, S.; Hunsom, M., Preparation of a High-Performance Pt–Pd/C-Electrocatalyst-Coated Membrane for ORR in PEM Fuel Cells Via a Combined Process of Impregnation and Seeding: Effect of Electrocatalyst Loading on Carbon Support. *Electrochim. Acta* **2011,** *56* (3), 1164-1171.
54. Antolini, E.; Giorgi, L.; Pozio, A.; Passalacqua, E., Influence of Nafion Loading in the Catalyst Layer of Gas-Diffusion Electrodes for PEFC. *J. Power Sources* **1999,** *77* (2), 136-142.
55. Rho, Y. W.; Srinivasan, S.; Kho, Y. T., Mass Transport Phenomena in Proton Exchange Membrane Fuel Cells using O_2 / He , O_2 / Ar , and O_2 / N_2 Mixtures: II . Theoretical Analysis. *J. Electrochem. Soc.* **1994,** *141* (8), 2089-2096.
56. Mayrhofer, K. J. J.; Strmcnik, D.; Blizanac, B. B.; Stamenkovic, V.; Arenz, M.; Markovic, N. M., Measurement of Oxygen Reduction Activities via the Rotating Disc Electrode Method: From Pt Model Surfaces to Carbon-Supported High Surface Area Catalysts. *Electrochim. Acta* **2008,** *53* (7), 3181-3188.

57. Elezović N.R., B. B. M., Vračar LJ.M., Krstajić N.V., Oxygen Reduction at Platinum Nanoparticles Supported on Carbon Cryogel in Alkaline Solution. *J. Serb. Chem. Soc.* **2007,** *72* (7), 699-708.
58. Huang, J. C.; Sen, R. K.; Yeager, E., Oxygen Reduction on Platinum in 85% Orthophosphoric Acid. *J. Electrochem. Soc.* **1979,** *126* (5), 786-792.
59. Maoka, T., Electrochemical Reduction of Oxygen on Small Platinum Particles Supported on Carbon in Concentrated Phosphoric Acid—II. Effects of Teflon Content in the Catalyst Layer and Baking Temperature of the Electrode. *Electrochim. Acta* **1988,** *33* (3), 379-383.
60. Zamora, H.; Cañizares, P.; Rodrigo, M. A.; Lobato, J., Improving of Micro Porous Layer based on Advanced Carbon Materials for High Temperature Proton Exchange Membrane Fuel Cell Electrodes. *Fuel Cells* **2015,** *15* (2), 375-383.
61. Lobato, J.; Zamora, H.; Plaza, J.; Cañizares, P.; Rodrigo, M. A., Enhancement of High Temperature PEMFC Stability using Catalysts based on Pt Supported on SiC based Materials. *Appl. Catal., B* **2016,** *198*, 516-524.
62. Mamlouk, M.; Scott, K., An Investigation of Pt Alloy Oxygen Reduction Catalysts in Phosphoric Acid Doped PBI Fuel Cells. *J. Power Sources* **2011,** *196* (3), 1084-1089.
63. Yao, J. H.; Elder, K. R.; Guo, H.; Grant, M., Theory and Simulation of Ostwald Ripening. *Phys. Rev. B* **1993,** *47* (21), 14110-14125.
64. Ham, H.; Park, N.-H.; Kim, S. S.; Kim, H. W., Evidence of Ostwald Ripening During Evolution of Micro-Scale Solid Carbon Spheres. *Sci. Rep.* **2014,** *4*, 3579.

Graphical Abstract